Count-rate Variations with Orientation of Camera Detector

S. M. Jahangir, A. B. Brill, Y. J. C. Bizais, and R. W. Rowe

Brookhaven National Laboratory, Upton, New York

Variations of count rate with orientation of the detector were investigated. Scaled difference images (SDI) were generated from pairs of arrays acquired at different detector orientations. The hypothesis tested was that any variations could be totally explained by random disintegration noise. We accepted or rejected this hypothesis according to the statistical significance of the difference between the measured and theoretical means and variances of the SDIs. When two images acquired at the same angle were compared, no significant differences were noted. Differences were significant between most pairs of images obtained at different angular orientations. Cameras with inadequate magnetic shielding were more sensitive to orientation effects than those with proper magnetic shielding. The mode of variation strongly suggests an interaction with a magnetic field

J Nucl Med 24: 356–359, 1983

The Anger camera has become the detector of choice for most conventional nuclear medicine imaging studies, and more recently for rotational tomography. For quantitative imaging it is necessary to compensate for the effects of detector nonuniformity (*1*) and nonlinearity (*2*). Emission computerized tomography places additionally stringent requirements on the stability of camera response (*3*), since small distortions can be greatly magnified by the reconstruction process. Recently it has been reported (*3*) that a change in a detector's orientation may cause variations in the image that cannot be attributed to mechanical deformations of the phantom. Thus any quantitative comparison of two images should take into account the relative detector orientations.

In this work we attempted to ascertain whether there were statistically significant differences between Anger-camera images acquired at different angular orientations, and if so, whether such differences could be attributed to an interaction with the earth's magnetic field.

METHOD

A "checkerboard" line phantom with 19 lines in both horizontal and vertical directions, was constructed from two narrow-bore, plastic tubes of 1.14-mm internal diameter. The grid lines were separated from each other by 2.83 cm. The phantom was filled with 5 mCi of Tc-99m and then clamped securely on top of the camera's collimator. Figure 1 shows the imaged pattern of this grid phantom as acquired by an Anger camera with a large field of view. In order to examine the effects of camera orientation on image quality, images were obtained at 30° angular intervals as the camera was rotated through 360°. Two principal types of rotation were performed as illustrated in Fig. 2. In type 1 rotation the camera's crystal was parallel to and facing away from the camera stand, with the axis of rotation perpendicular to the camera face. During type 2 rotation the camera face was perpendicular to the stand and parallel to the axis of rotation. This latter mode is similar to the orientation sequence used in rotational tomography. If, in either mode of rotation, the axis of rotation was aligned east-west, we coded this as type 1EW or type 2EW rotation. Similarly type 1NS and type 2NS refer to type 1 and type 2 rotations with the axis of rotation aligned north-south.

The experiment was carried out on four different Anger cameras, two of which (cameras I and II) have proper Mu metal magnetic shielding around each photomultiplier tube, the other

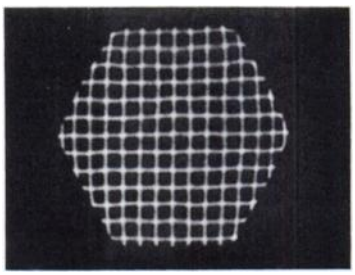

FIG. 1. 1000-K count image of checkerboard line phantom.

Received Sept. 24, 1982; revision accepted Jan. 3, 1983.

For reprints contact: A. B. Brill, MD, PhD, Medical Dept, Brookhaven Laboratory, Upton, New York 11973.

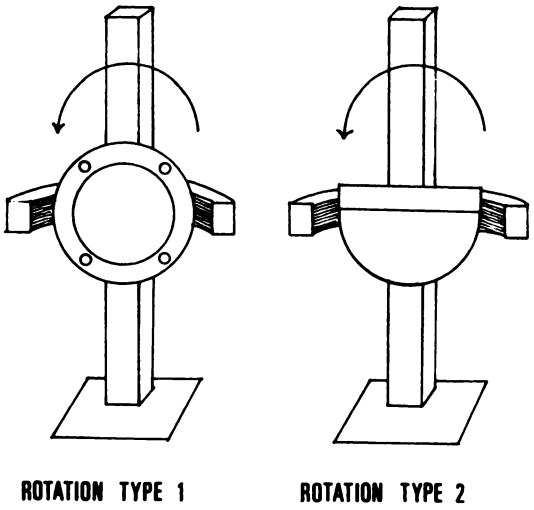

FIG. 2. Rotation modes used to investigate image variations with camera orientation. In type 1 rotation, the camera-crystal was parallel to and facing away from camera stand, with axis of rotation perpendicular to camera face. For type 2 rotation, camera face was perpendicular to stand and parallel to axis of rotation.

two (cameras III and IV) have inadequate magnetic shielding (camera III had none, and camera IV had incomplete photomultiplier tube coverage near the photocathodes). Successive images were acquired with a 20% symmetrical energy window, at angular intervals of 30° with a one-min pause between the end of one frame and the start of the next, during which the rotation took place. Each image was collected for 3 min into a 256 × 256 matrix in byte mode, as part of a multiple static study under software.* In addition, a similar series of successive frames was acquired without rotation of the camera, with the camera face parallel to the ground and facing up.

ANALYSIS

To compare the images at different orientations a hypothesis was assumed such that any differences between images could be totally explained by the random disintegration noise and the decay process. It was thus assumed that the imaged phantom and the characteristics of the Anger cameras did not change. The hypothesis leads to the definition of a scaled difference image (SDI) between two images given by

$$d(i) = (m_1(i) - m_2(i)) \Big/ \left(\frac{m_1(i) + m_2(i)}{2}\right)^{1/2}$$

where $m_1(i)$ and $m_2(i)$ are the i^{th} pixel content of the first and second images respectively. In other words the SDI is the difference between the two images divided by the mean standard deviation of the two images. If the hypothesis is true then this SDI will be distributed as a Gaussian function with variance 2 and mean D asymptotically equal to

$$D = 2\left(\frac{1 - \exp(-\lambda\Delta)}{1 + \exp(-\lambda\Delta)}\right) E\left(\frac{m_1(i) + m_2(i)}{2}\right)^{1/2},$$

where $E(\cdot)$ denotes the expectation operator, λ the decay constant and, Δ the time lag between the beginning of two acquisitions.

The estimated variance and mean were also calculated for each recorded SDI. When the difference between the estimated and theoretical values was statistically significant at a level of 1% error of the first kind, the hypothesis was rejected. Two tests for normality were carried out from estimates of skewness and kurtosis while estimated mean and variance were tested against the theoretical values.

RESULTS AND DISCUSSION

The SDIs showed no significant differences when the cameras were not rotated. However, significant differences between the images at 30° intervals appeared when the detectors were subjected to type 1 and type 2 rotations. Cameras I and II yielded very similar results, whereas cameras III and IV behaved like each other but considerably differently from cameras I and II. Figures 3 and 4 show isometric representations of the checkerboard line images obtained with camera I and camera III respectively, at four different angular orientations during type 2EW rotation. No obvious differences were seen between the four images acquired with camera I. However, gross visual variations with angle were observed in the images obtained with camera III. In type 1 rotation, however, these differences were not so great and did not vary with geographical alignment of the axis of rotation. Figure 5 shows the SDIs between frames at 0° and 90°, 0° and 180° and 0° and 270°

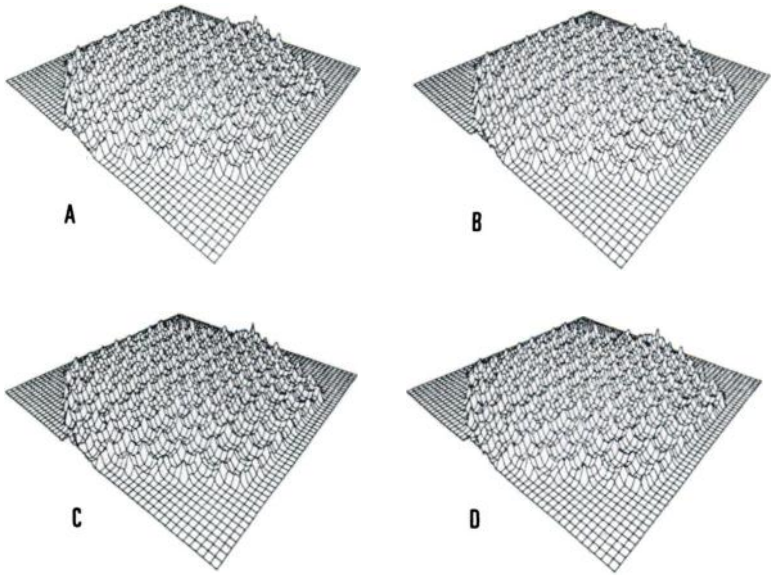

FIG. 3. Isometric representations of checker-board line images for camera I at 0° (A), 90° (B), 180° (C), and 270° (D) for type 2EW rotation.

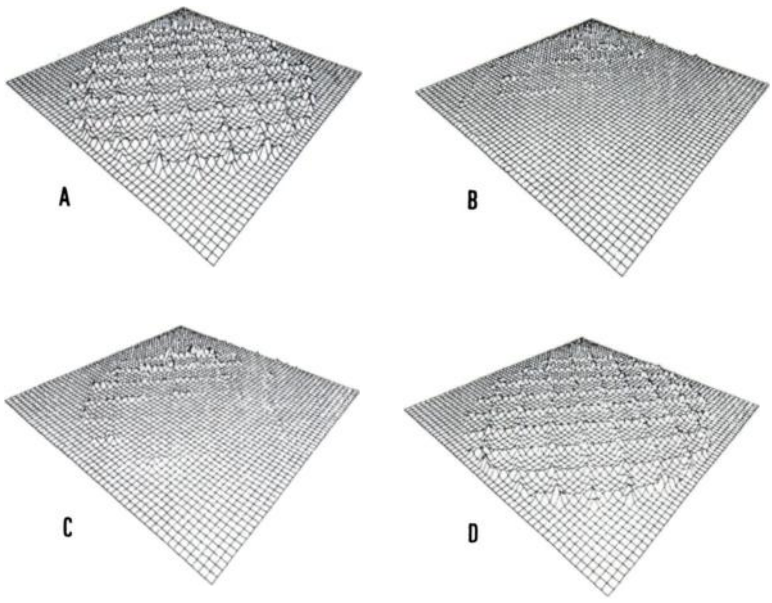

FIG. 4. Isometric representations of checker-board line images for camera III at 0° (A), 90° (B), 180° (C), and 270° (D) for type 2EW rotation.

for camera I (images D,E,F) and camera III (images A,B,C) in type 1 rotation. The scaled differences were much smaller for camera I than for camera III, and appeared to be fairly randomly distributed in all three SDIs. On the other hand, the SDIs for camera III varied with orientation and displayed structure similar to that of the phantom itself.

Figures 6 and 7 display statistical parameters of images acquired by cameras I and III respectively. The upper graphs plot the differences between estimated and theoretical means (DEMTM) of the SDIs for successive frames, and the lower plots show the corresponding differences between estimated and theoretical variances (DEVTV). On the left-hand side, these parameters are displayed for sequential camera frames without rotation while on the right-hand side, the frame numbers correspond to successive 30° intervals during type 2EW rotation. Points in the graphs lying above the dashed lines represent significant differences at a level of 1% error.

When there was no rotation of the camera the differences were not significant except in the case of DEVTV for camera III. However, when the flood field corrector circuit was turned off, the differences for this camera were no longer significant (lower curve Fig. 7c). The corrector circuit in camera I did not affect the significance of the differences between theoretical and estimated means and variances. Figures 6b and 6d show that statistically significant image variations occurred with the rotation of camera I, although these were not easily distinguishable in the original phantom images. During rotation of camera III, highly significant variations occurred in both DEMTM and DEVTV (Figs. 7b and 7d). In type 2NS rotation, less significant variations were observed, though they were still well above the 1% confidence limit.

Type 2 rotation causes the camera photomultiplier tube to make different angles with the direction of the earth's magnetic field at each camera orientation. Thus, in the absence of magnetic shielding, orientation-dependent accelerations would be imparted to the electrons traveling through the photomultiplier tubes, which would result in varying image distortions with angle. In type 1 rotation, the photomultiplier tubes always maintain the same orientation with respect to the earth's magnetic field. Only a very small angle dependence of distortions would therefore be expected in this mode of rotation. The most significant variations between images were observed in type 2 rotation of cameras with little or no magnetic shielding.

CONCLUSION

Large orientation-dependent variations in image quality were observed in cameras with inadequate magnetic shielding. Caution is thus advised in in the use of such cameras—for example, in a comparison between images obtained at different times where the orientation of the camera may have changed between acquisitions. Furthermore, even in cameras with good magnetic shielding, significant changes in images were measured during a rotation se-

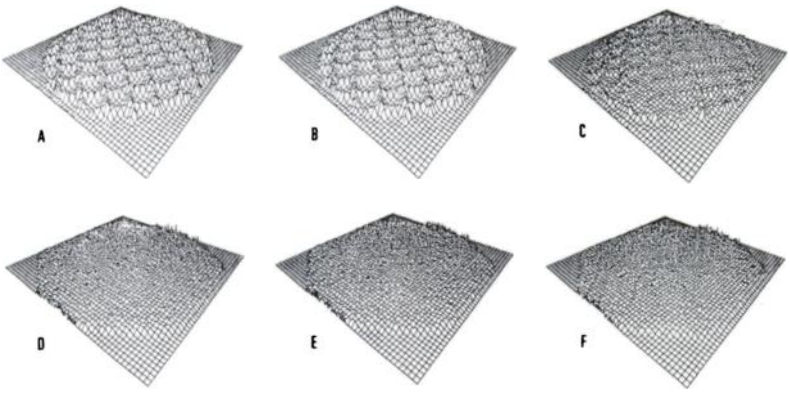

FIG. 5. Isometric representations of SDIs for camera III (images A,B and C) and camera I (images D,E and F) at 0° and 90° (A,D), 0° and 180° (B,E) and 0° and 270° (C,F) in type 1 rotation

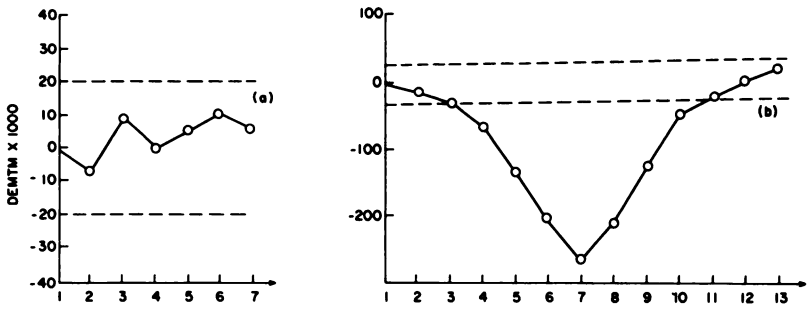

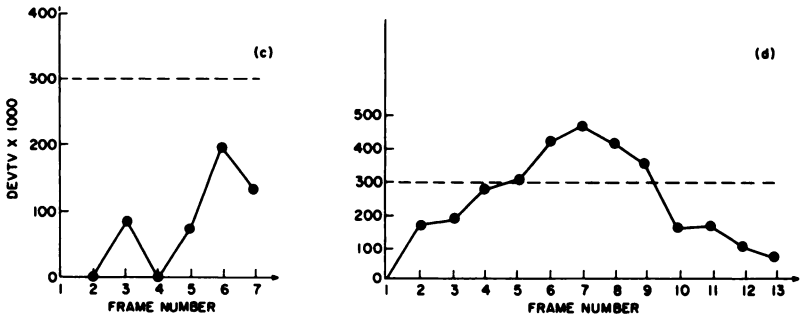

FIG. 6. Curves of statistical parameters of images acquired by camera I for type 2EW rotation. Upper graphs (a,b) plot differences between estimated and theoretical means (DEMTM), and lower graphs (c,d) plot differences between estimated and theoretical variances (DEVTV), against frame numbers. In left-hand graphs sequential frames were obtained without rotation of camera. Successive frames in right-hand plots represent images at 30° intervals.

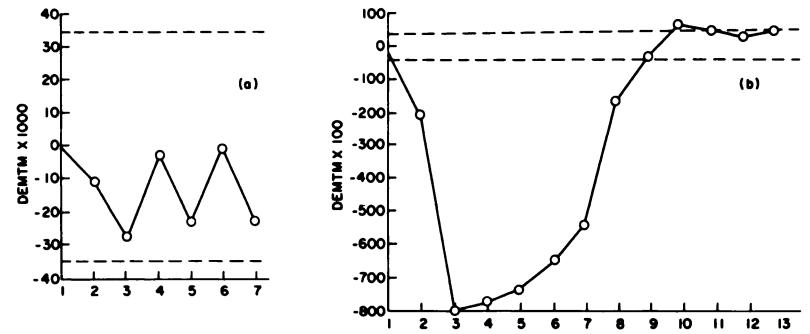

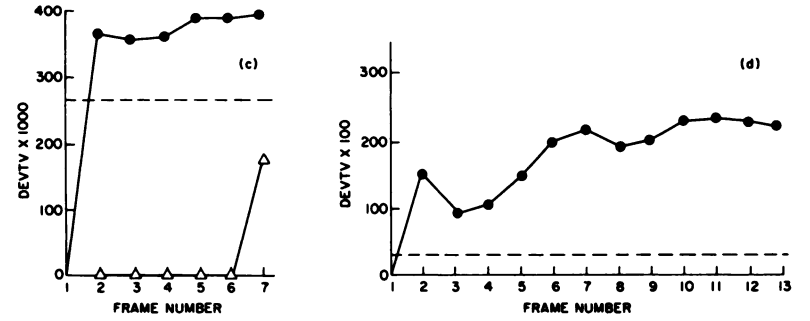

FIG. 7. Curves of statistical parameters of images acquired by camera III for type 2EW rotation. Upper graphs (a,b) plot DEMTM and lower graphs (c,d) plot DEVTV against frame numbers. Graphs with triangular points in (c), display results with corrector circuit off. In left-hand pair, sequential frames were obtained without rotation of camera. Successive frames in right-hand pair represent images at 30° intervals.

quence similar to that used in tomography. Since very small distortions in the projection images can be amplified to an unacceptable level by the reconstruction process, the magnitude of the rotation effects observed suggests that considerable attention must be paid to the magnetic shielding of cameras that are to be used for rotational tomography. Also, correction for rotation-dependent distortion may be necessary for quantitative tomographic imaging with Anger cameras.

FOOTNOTE

* DEC Gamma-11.

ACKNOWLEDGMENTS

Research supported under Contract No. DE-AC02-76CH00016 with the U.S. Department of Energy and IAEA project contract No. 2572/RB. By acceptance of this article, the publisher and/or recipient acknowledges the U.S. Government's right to retain a nonexclusive, royalty-free license in and to any copyright covering this paper.

REFERENCES

1. TODD-POKROPEK A, ZUROWSKI S, SOUSSALINE F: Nonuniformity and artifact creation in tomography. *J Nucl Med* 21:P38, 1980
2. KNOLL GF, BENNETT MC, KORAL KF, et al: Removal of gamma camera nonlinearity and nonuniformities through real-time signal processing. *Proceedings of the Conference on Information Processing in Medical Imaging. INSERM* 88: 187-200, 1979
3. ROGERS WL, CLINTHORNE NH, HARKNESS BA, et al: Field-flood requirements for Emission Computed Tomography with an Anger-Camera. *J Nucl Med* 23:162-168, 1982